Simulations of Atmospheric General Circulations of Earth-like Planets by AFES

Project Representative

Yoshi-Yuki Hayashi   Department of Earth and Planetary Sciences, Kobe University

Authors

Yoshi-Yuki Hayashi   Department of Earth and Planetary Sciences, Kobe University
Yoshiyuki O. Takahashi   Department of Earth and Planetary Sciences, Kobe University
Norihiko Sugimoto   Research and Education Center for Natural Sciences, Keio University
Masahiro Takagi   Faculty of Science, Kyoto Sangyo University
Hiroki Kashimura   Institute of Space and Astronautical Science, Japan Aerospace Exploration Agency
Masaki Ishiwatari   Department of Cosmosciences, Hokkaido University
Masatsugu Odaka   Department of Cosmosciences, Hokkaido University
Kensuke Nakajima   Department of Earth and Planetary Sciences, Kyushu University
George L. Hashimoto   Department of Earth Sciences, Okayama University
Yoshihisa Matsuda   Faculty of Education, Tokyo Gakugei University

High resolution simulations of the Venus and Mars atmospheres have been performed by using a General Circulation Model (GCM) based on AFES (Atmospheric GCM for the Earth Simulator). Our aim is to have insights into the dynamical features of small and medium scale disturbances in the Earth-like atmospheres and their roles in the general circulations. As for the simulation of the Venus atmosphere, a superrotation is reasonably reproduced with a realistic solar heating. Spectral analyses of the horizontal kinetic energy are performed for the high-resolution case (T159L120). The results suggest that small-scale gravity waves might be more important in Venus than in Earth. In addition, the structure of a polar vortex in a simulation is investigated to compare with observations. The "S-shaped" horizontal structure and vertical profile of the polar vortex is successfully reproduced. Based on the previous linear stability analyses, the dependence of the appearance of baroclinic instability on the meridional profile of zonal flow and the vertical profile of static stability is investigated. The results suggest that the realistic vertical distribution of static stability and a sufficiently high horizontal resolution are crucial for the occurrence of baroclinic instability. The results also indicate that baroclinic instability contributes significantly to the general circulation of the Venus atmosphere when the zonal mean flow, as is often observed, is characterized by the appearance of the mid-latitude jets. As for the simulation of the Martian atmosphere, the nature of dust lifting in the model is investigated by performing multiple runs with several horizontal resolutions from T79 to T639. The model demonstrates a variety of disturbances whose horizontal scales range from synoptic scales to tens of kilometers. The analyses of dust lifting events in terms of probability distribution function indicate that dust lifting amount, in general, increases with the increase of the resolution owing to the better representation of small scale disturbances in the higher resolution model. However, especially in the mid- and high-latitudes, dust lifting amount in the lower resolution model is sometimes larger than that in the higher resolution model. This inverse dependence of dust lifting amount would be a reflection of the large variability of synoptic eddies in those latitudes compared to the small scale disturbances in the lower latitudes.

Keywords: planetary atmospheres, superrotation, dust storm, Earth, Mars, Venus

1. Introduction

The structure of the general circulation differs significantly in each of the planetary atmospheres. For instance, the atmospheres of the slowly rotating Venus and Titan exemplify the states of superrotation where the equatorial atmospheres rotate faster than the solid planets beneath, while the equatorial easterly and the strong mid-latitude westerly jets form in the Earth's troposphere. The global dust storm occurs in some years on Mars, but a similar storm does not exist in the Earth's atmosphere. Understanding physical mechanisms causing such a variety of features in the general circulations of the planetary atmospheres is one of the most interesting and important open questions of the atmospheric science and fluid dynamics.

The aim of this study is to understand dynamical processes that characterize the structure of each planetary atmosphere by performing simulations of those planetary atmospheres by

using GCMs with a common dynamical core of AFES [1]. Appropriate physical processes are adopted for each planetary atmosphere. In the followings, the particular targets of each simulation, the physical processes utilized, and the results obtained will be described briefly.

2. Venus simulation

2.1 Targets of simulations

Low-resolution general circulation models have been used to simulate the superrotation of the Venus atmosphere in precedent studies, such as Yamamoto and Takahashi [2]. This is mainly due to the extremely long spin-up time needed to generate a superrotation from a motionless initial state. Furthermore, most of previous GCM studies included unrealistically intense solar heating and large static stability to generate a superrotation. In the present study, we construct a new model based on AFES for realistic high-resolution simulations of the Venus atmosphere.

Kinetic energy spectra have been utilized to explore properties of disturbances of a wide range of scales both in observational and numerical studies of the Earth atmosphere [3, 4]. As for the Venus atmosphere, it is suggested from observational studies such as Leroy and Ingersoll [5] that small-scale gravity waves play important roles at the cloud levels. However, kinetic energy spectra of the Venus atmosphere have not been well described yet. At the polar region of the Venus atmosphere, a strong polar vortex having "S-shaped" structure has been frequently observed by VIRTIS onboard Venus Express [6]. However, there has been no numerical simulation which reproduces such a polar vortex with a good agreement with observational studies so far. Our Venusian AFES with realistic solar heating and static stability profiles has successfully reproduced a reasonable superrotation. In this fiscal year, we perform simulations with very high resolutions to investigate properties of disturbances in a wide range of scales in the Venus atmosphere. The "S-shaped" structure of the Venus polar vortex is one of the targets which a high resolution model may represent. We conducted several sensitivity tests on baroclinic instability by AFES in the last year [7]. In this fiscal year, we investigate, consulting the previous linear stability analyses [8, 9], dependence of baroclinic instability on the choice of the basic state, i.e. the meridional profile of zonal flow and the vertical profile of static stability.

2.2 Model and experimental settings

Venus simulations are performed with simplified physical processes adopting the values of physical constants appropriate for Venus. The experimental settings basically follow those of the previous linear stability analysis [9] and the AFES simulations conducted last year [7]. The highest resolution used in the present simulations is T159L120, which is equivalent to about 79 km horizontal grid size. The vertical domain extends from the ground to about 120 km with almost the constant grid spacing of 1 km. Simulations with T63L120 and T42L60 resolutions, which are equivalent to about 198 km horizontal grid size and 120 vertical layers and about 297 km horizontal grid size with 60 vertical layers, respectively, are also performed.

The physical processes adopted in the model are vertical eddy diffusion with a constant diffusion coefficient of 0.15 m^2/s, a dry convective adjustment, the Newtonian cooling, and the Rayleigh friction at the lowest level representing the surface friction. In the upper region above about 80 km, a sponge layer is assumed; the friction increasing gradually with altitude acts to damp the eddy component only. In addition, the model includes a 4th-order horizontal diffusion (∇^4) with an e-folding time for the maximum wavenumber of about 0.01 days for T159, 0.03 days for T63, and 0.1 days for T42 simulations. The coefficients of the Newtonian cooling are based on the previous study [10]. The equilibrium temperature distribution toward which temperature is relaxed by the Newtonian cooling is the initial field described below. We adopt a realistic profile of solar heating. The vertical profile of solar heating is based on the previous works [10, 11]. Several solar heating distributions are used for simulations: a zonally averaged solar heating distribution, a diurnally varying solar heating distribution, and no solar heating.

For almost all simulations described below, the vertical temperature profiles of the initial conditions are constructed based on the observed vertical distribution of static stability [12]. In this temperature profile, the lower atmosphere near the ground is weakly stable. Below the cloud layer, static stability has a maximum at around 45 km. A layer with almost neutral stability exists from 55 to 60 km representing the cloud layer influenced by solar heating. Above the cloud layer (above 70 km), it is strongly stratified. Meridional temperature gradient from equator to pole is about 5 K on the model level, i.e., constant sigma surface, at the top of cloud layer. The initial condition for wind velocity is zonally symmetric, solid-body superrotating flow, which is determined by the gradient wind balance; zonal velocity at the equator linearly increases from zero at the ground up to 100 m/s at the altitude of 70 km, and above there the atmosphere is in a solid-body rotation with the same speed as that at 70 km. From this initial condition, time integration is performed for four Earth years.

In addition, for the investigation of dependence of baroclinic wave intensity on the basic state, we prepare a relatively realistic profile of zonally uniform zonal flow with mid-latitude jets near the cloud levels.

2.3 Results

In the results of the numerical simulation in which solar heating is excluded for simplicity, the zonal wind velocity decreases a little from the initial condition in the cloud layer (50-70 km) due to unstable modes of growing vortices. The preliminary results without solar heating are summarized in

Sugimoto et al. [7].

Fig. 1 shows snapshots of vorticity deviation from its zonal mean (left) and temperature (right) at 54 km altitude at 1422 days from the initial condition of the T159L120 simulation with the diurnally varying solar heating. A vortical structure appears at the mid-latitudes where meridional temperature gradient is large. Small filament structures of vorticity appear around the large-scale vortices. In addition, small-scale vortical disturbances are produced by the intense thermal forcing around the equatorial region. The temperature gradient produced by the thermal forcing enhances meridonal circulation and then the strong mid-latitude jets appear. On the other hand, strong meridional gradients of velocity and temperature generate baroclinic and barotropic unstable waves continuously. These instabilities would be the source of small-scale disturbances.

We calculate the horizontal kinetic energy spectrum [13] for the result of T159L120 simulation with the diurnally varying solar heating. Fig. 2a shows the horizontal kinetic energy spectra at eight sigma levels averaged over the last one year of the integration. The energy spectra obey $-5/3$ power law in the range of $10 < n < 40$, where n is the total wavenumber. Further,

the horizontal kinetic energy is decomposed into a rotational component showing the contribution of balanced motion (e.g., Rossby waves) and a divergent component showing that of unbalanced motion (e.g., gravity waves); both components are displayed in Figs. 2b and c. The spectrum of the rotational component at $\sigma = 0.03$ (~ 40 km) shows -3 power law for $n < 20$; whereas the spectra in the other levels are gentler than -3 power law but steeper than $-5/3$ one. The divergent component in the upper two levels shows $-5/3$ power law extending to very small wavenumbers (planetary scales). The ratios of the divergent component to the rotational one for each level are also examined. For $n > 10$, the divergent component is comparable to rotational component or dominant. The dominance of the divergent component even in low wavenumbers might be a unique feature of the Venus atmosphere.

Fig. 3 shows time evolution of vorticity at 62 km altitude in the polar region for the T42L60 simulation with the diurnally varying solar heating. The "S-shaped" structure is successfully reproduced. The dominant wavenumber varies from two to three. We also investigate the vertical structure of phase for the wavenumber one component. The phase is anti-symmetric about
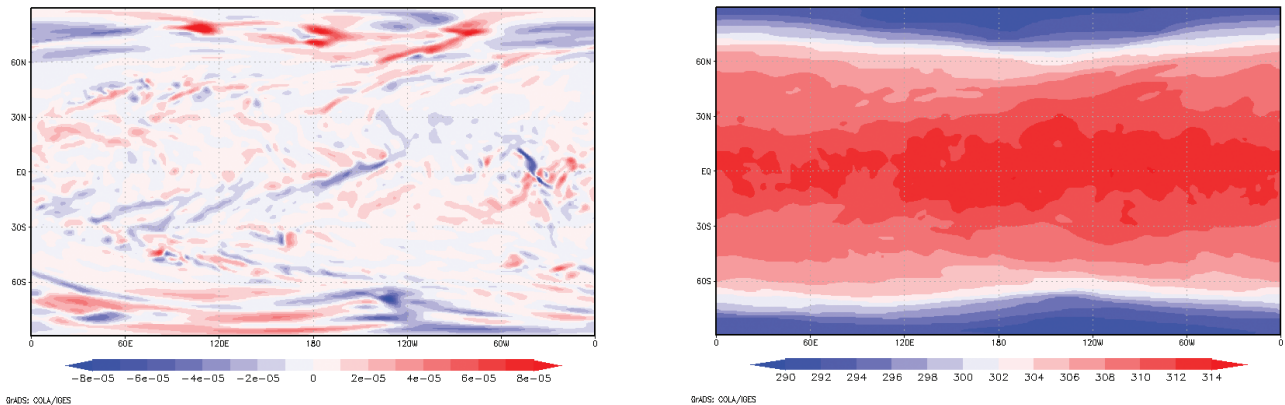

Fig. 1 Snapshots of distributions of vorticity deviation from its zonal mean (left) and temperature (right) at 54 km altitude and at 1422 days from the initial condition of the T159L120 simulation with the diurnally varying solar heating.
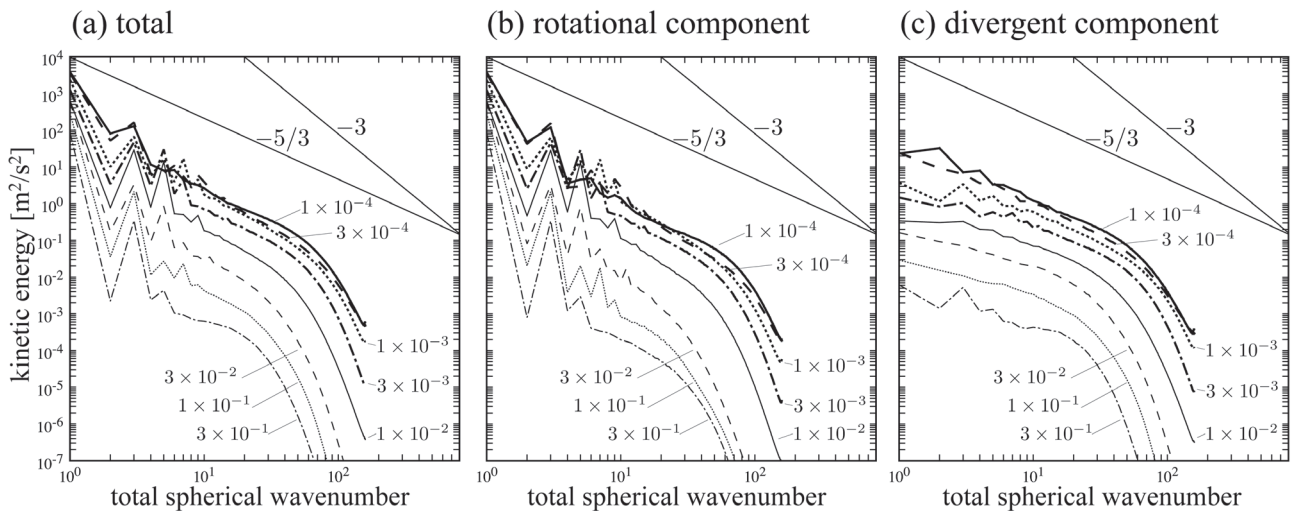

Fig. 2 Horizontal kinetic energy spectra of (a) total, (b) rotational component, and (c) divergent component. Two straight lines in each panel show slopes of -3 power law and $-5/3$ power law, respectively.
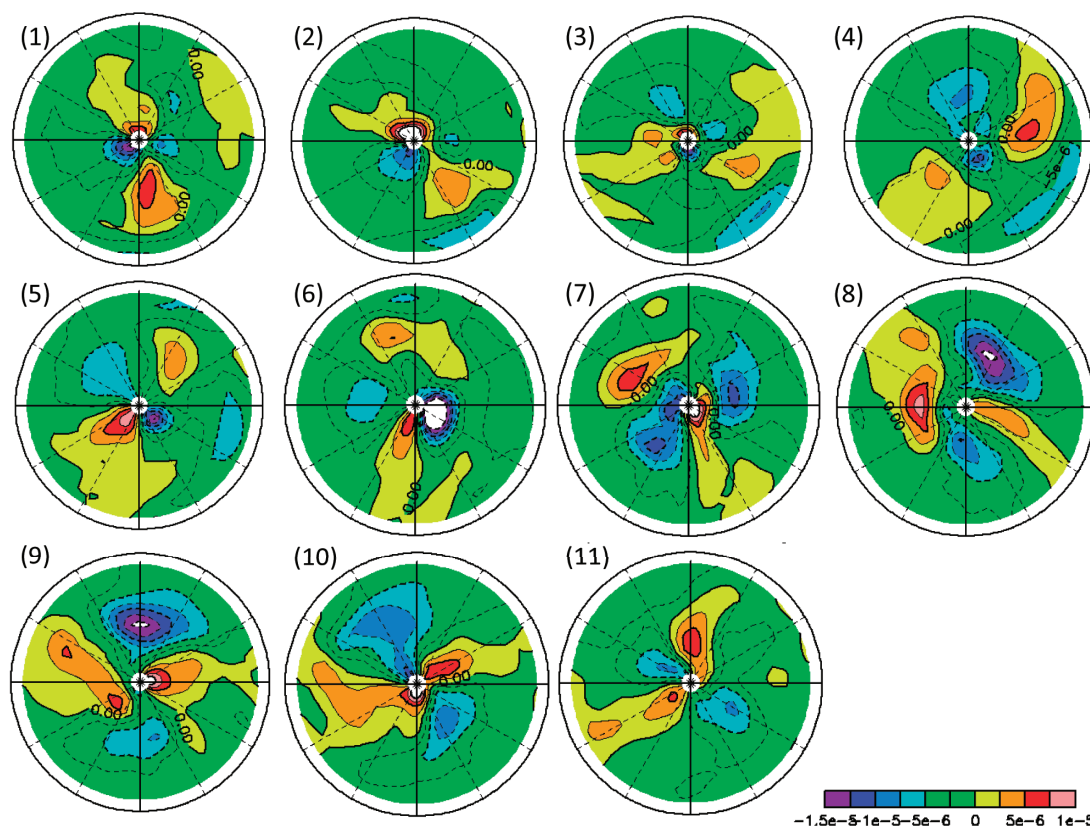
Fig. 3 Time evolution of vorticity at 62 km altitude in the polar region (60°N−90°N) from (1) t = 1365 days to (11) t = 1375 days. Time interval between panels is 12 hours.

at 62 km altitude (figures are not shown here) where the static stability and the vertical shear change strongly. These results agree well with observational studies. Our model can reproduce the polar vortex of the Venus atmosphere self-consistently; and further analysis will reveal dynamics of the polar vortex.

We also conduct sensitivity tests to explore the dependence of baroclinic instability on the initial meridional profile of zonal flow, on the vertical profile of static stability for the Newtonian cooling, and on the model resolution. The results indicate that the realistic vertical distribution of static stability and a sufficiently high resolution are crucial for the occurrence of baroclinic instability (figures are not shown here). The results also indicate that baroclinic instability contributes significantly to the general circulation of the Venus atmosphere when the zonal mean flow, as is often observed, is characterized by the appearance of the mid-latitude jets. The results of the sensitivity tests are summarized in Sugimoto et al. [14].

3. Mars simulation

3.1 Targets of simulations

Radiative effect of dust suspended in the Martian atmosphere has important impacts on the thermal and circulation structure of the Martian atmosphere. However, it has not been well understood what kind of dynamical phenomena play important roles in lifting dust from the ground into the atmosphere. A previous study by using a Mars GCM [15] suggests that the effects of subgrid scale wind fluctuations caused by small and medium scale disturbances would be important for the dust lifting processes. However, the features of small and medium scale disturbances which may contribute to the dust lifting have not been revealed yet. Disturbances of these scales are not easy to be observed and to be resolved in numerical models. In order to examine the disturbances in the Martian atmosphere and its effects on dust lifting, we have been performing medium and high resolution simulations of Martian atmosphere by using our Martian AFES. In this fiscal year, properties of dust lifting are analyzed in terms of probability distribution function.

3.2 Model and experimental settings

Mars simulations are performed with the AFES including physical processes introduced from the Mars GCM [16, 17] which has been developed in our group, and with the values of physical constants appropriate for the Mars. The implemented physical processes are radiative, turbulent mixing, and surface processes. By the use of this model, several simulations are performed. Resolutions of simulations are T79L96, T159L96, T319L96, and T639L96, which are equivalent to about 89, 44, 22, and 11 km horizontal grid sizes, respectively. In the simulations, the atmospheric dust distribution is prescribed, and the dust is uniformly distributed in horizontal direction with an amount corresponding to visible optical depth of 0.2. However, the dust lifting parameterization [18] is included in the model to diagnose the possible amount of dust lifting.

3.3 Results

Fig. 4 and 5 show snapshots of distribution of relative vorticity at 4 hPa pressure level and dust lifting flux during the northern fall from the T639L96 simulation. It is shown that a lot of disturbances with a variety of horizontal scales are responsible for dust lifting in the model. Most intense dust lifting occurs associated with synoptic scale eddies around the northern polar cap edge. At the same time, small scale eddies also contribute to dust lifting. Some of those are associated with small and medium scale orographic variations, but others are not.

Here, the nature of resolution dependence of dust lifting events in the model is examined in terms of probability distribution function. Fig. 6 shows the probability distribution function of dust lifting flux as a function of surface stress. It is found that dust lifting flux, in general, increases with increasing resolution over almost all surface stress values. However, as is shown in Fig. 6, in our simulation, the dust lifting flux from T159L96 simulation is larger than that in T319L96 simulation. Fig. 7 and 8 show the same as Fig. 6, but for two latitudinal bands. It is shown that dust lifting flux increases with increasing resolution in the region from 60ºS to 30ºN, where small scale vortices appear. But, in the region south of 60ºS and north of 30ºN, the dust lifting flux from T159L96 simulation is larger

than those from the higher resolution simulations. The dust lifting events in mid- and high-latitudes are mainly caused by synoptic eddies as is shown in Fig. 4. It is implied that a variability of synoptic eddies in mid- and high-latitude would contaminate the resolution dependence of dust lifting.

Fig. 6 Probability distribution function of dust lifting flux as a function of surface stress at northern fall with the resolutions of T639L96, T319L96, T159L96, and T79L96.

Fig. 7 Same as Fig. 6, but for probability distribution function at the region from 60ºS to 30ºN.
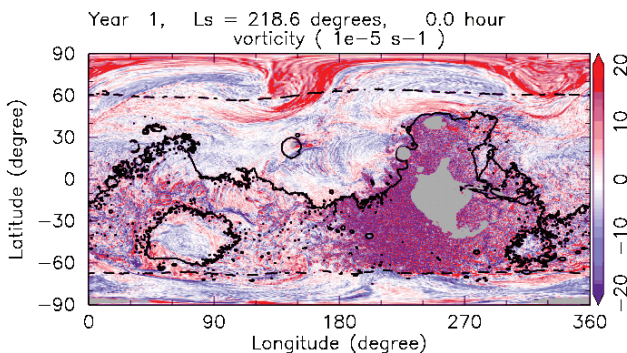

Fig. 4 Global distribution of vorticity at 4 hPa pressure level at northern fall with the resolution of T639L96. Unit of vorticity is 10^{-5} s^{-1}. Also shown is the areoid (solid line) and low latitude polar cap edge (dashed line). Gray areas represent mountains at the 4 hPa pressure level.
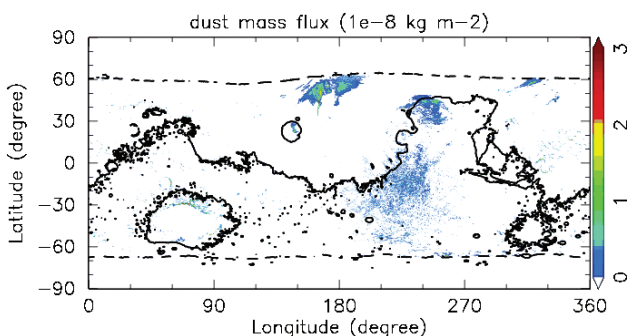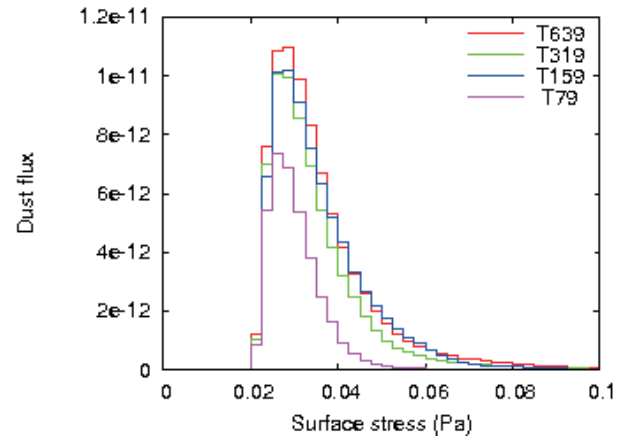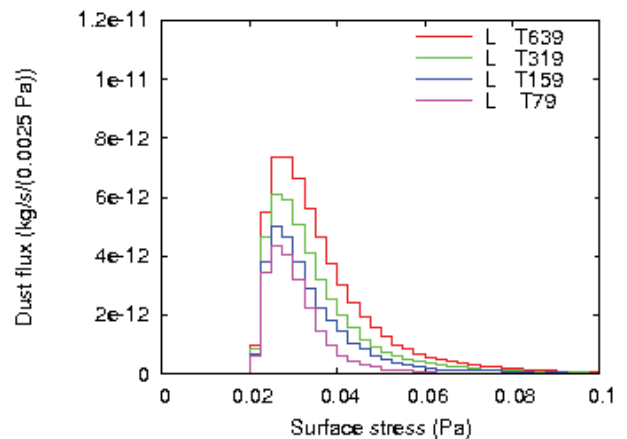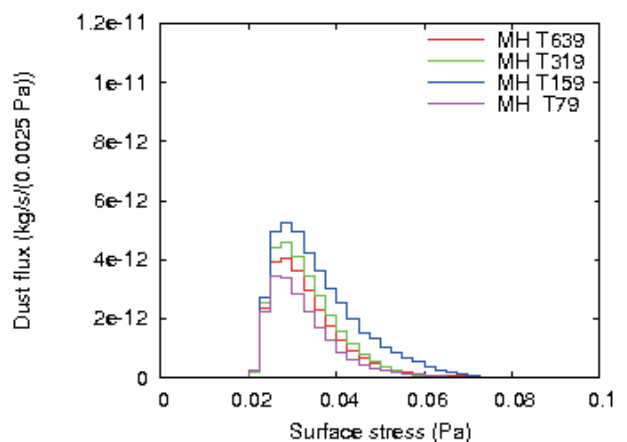

Fig. 5 Same as Fig. 4, but for dust lifting flux at the ground. Unit of dust lifting flux is arbitrary.

Fig. 8 Same as Fig. 6, but for probability distribution function at the region south of 60ºS and north of 30ºN.

References

[1] Ohfuchi, W., H. Nakamura, M. K. Yoshioka, T. Enomoto, K. Takaya, X. Peng, S. Yamane, T. Nishimura, Y. Kurihara, and K. Ninomiya, "10-km Mesh Meso-scale Resolving Simulations of the Global Atmosphere on the Earth Simulator - Preliminary Outcomes of AFES (AGCM for the Earth Simulator) –", Journal of the Earth Simulator, 1, 8, 2004.

[2] Yamamoto, M. and M. Takahashi, "The fully developed superrotation simulated by a general circulation model of a Venus-like atmosphere", J. Atmos. Sci., 60, 561-574, 2003.

[3] Nastrom, G. D. and K. S. Gage, "A climatology of atmospheric wavenumber spectra of wind and temperature observed by commercial aircraft", J. Atmos. Sci., 42, 950–960, 1985.

[4] Takahashi, Y. O., K. Hamilton, and W. Ohfuchi, "Explicit global simulation of the mesoscale spectrum of atmospheric motions", Geophysical Research Letters, 33, L12812, doi:10.1029/2006GL026429, 2006.

[5] Leroy, S. S. and A. P. Ingersoll, "Radio scintillations in Venus's atmosphere: application of a theory of gravity wave generation", J. Atmos. Sci., 53, 1018-1028, 1996.

[6] Piccioni, G. et al., "South-polar features on Venus similar to those near the north pole", Nature, 450, 637-640, 2007.

[7] Sugimoto, N., M. Takagi, Y. Matsuda, Y. O. Takahashi, M. Ishiwatari, and Y.-Y. Hayashi, "Baroclinic modes in the atmosphere on Venus simulated by AFES", Theoretical and Applied Mechanics Japan, 61, 11-21, 2013.

[8] Young, R. E., H. Houbel, and L. Pfister, "Baroclinic instability in the Venus atmosphere", J. Atmos. Sci., 41, 2310–2333, 1984.

[9] Takagi, M. and Y. Matsuda, "A study on the stability of a baroclinic flow in cyclostrophic balance on the sphere", Geophysical Research Letters, 33, L14807, doi:10.1029/2006GL026200, 2006.

[10] Crisp, D., "Radiative forcing of the Venus mesosphere: I. solar fluxes and heating rates", Icarus, 67, 484-514, 1986.

[11] Tomasko M. G., L. R. Doose, P. H. Smith, and A. P. Odell, "Measurements of the flux of sunlight in the atmosphere of Venus", J. Geophys. Res., Vol. 85, 8167-8186, 1980.

[12] Gierasch P. J., R. M. Goody, R. E. Young, D. Crisp, C. Edwards, R. Kahn, D. Rider, A. Del Genio, R. Greeley, A. Hou, C. B. Leovy, D. McCleese, and M. Newman, "The General Circulation of the Venus Atmosphere: an Assessment", In Venus II: Geology, Geophysics, Atmosphere, and Solar Wind Environment. University of Arizona Press, p.459, 1997.

[13] Koshyk, J. N. and K. Hamilton, "The horizontal kinetic energy spectrum and spectral budget simulated by a high-resolution troposphere-stratosphere-mesosphere GCM", J. Atmos. Sci., 58(4), 329–348, 2001.

[14] Sugimoto, N., M. Takagi, and Y. Matsuda, "Baroclinic instability in the Venus atmosphere simulated by GCM", J. Geophys. Res., under revision. (2014JE004624)

[15] Wilson, R. J. and K. Hamilton, "Comprehensive Model Simulation of Thermal Tides in the Martian Atmosphere", J. Atmos. Sci., 53, 1290-1326, 1996.

[16] Takahashi, Y. O., H. Fujiwara, H. Fukunishi, M. Odaka, Y.-Y. Hayashi, and S. Watanabe, "Topographically induced north-south asymmetry of the meridional circulation in the Martian atmosphere", J. Geophys. Res., 108, 5018, doi:10.1029/2001JE001638, 2003.

[17] Takahashi, Y. O., H. Fujiwara, and H. Fukunishi, "Vertical and latitudinal structure of the migrating diurnal tide in the Martian atmosphere: Numerical investigations", J. Geophys. Res., 111, E01003, doi:10.1029/2005JE002543, 2006.

[18] Newman, C. E., S. R. Lewis, and P. L. Read, "Modeling the Martian dust cycle 1. Representation of dust transport processes", J. Geophys. Res, 107, 5123, doi:10.1029/2002JE001910, 2002.

AFES を用いた地球型惑星の大気大循環シミュレーション

課題責任者

林　　　祥介　　　神戸大学　大学院理学研究科

著者

林　　　祥介　　　　　　　神戸大学　大学院理学研究科

高橋　芳幸　　　　　　　　神戸大学　大学院理学研究科

杉本　憲彦　　　　　　　　慶應義塾大学　自然科学研究教育センター

高木　征弘　　　　　　　　京都産業大学　理学部

樫村　博基　　　　　　　　宇宙航空研究開発機構　宇宙科学研究所

石渡　正樹　　　　　　　　北海道大学　大学院理学研究院

小高　正嗣　　　　　　　　北海道大学　大学院理学研究院

中島　健介　　　　　　　　九州大学　大学院理学研究院

はしもとじょーじ　　　　　岡山大学　大学院自然科学研究科

松田　佳久　　　　　　　　東京学芸大学　教育学部

　大気大循環モデル AFES（AGCM (Atmospheric General Circulation Model) for the Earth Simulator）に基づく GCM を用いて、金星および火星大気の高解像度大気大循環シミュレーションを実施した。我々の研究の目的は、地球型惑星大気における中小規模擾乱の力学的特徴と、その大気大循環への影響を調べることである。金星大気シミュレーションでは、現実的な太陽加熱を用いて長時間スーパーローテーションを維持することができた。その高解像度計算（T159L120）の結果を用いて水平運動エネルギーのスペクトル解析を行い、金星大気では小規模重力波が地球大気に比べてより重要である可能性を示唆した。また、モデル中に現れた極渦の構造を観測と比較し、S 字構造や鉛直構造が整合的であることを示した。さらに、基本場の安定度の鉛直構造と速度の水平構造に対する線形不安定解析の結果を基に、傾圧不安定の発現の依存性も調べた。その結果、傾圧不安定波の発達には現実的な安定度の鉛直分布とこれを表現する十分な解像度が必要であることを示し、観測で見られるような中緯度ジェットをもつ東西風の下では傾圧不安定波が金星大気大循環においてより重要な働きをもたらすことを予想させる結果を得た。火星大気シミュレーションでは、T79 から T639 までの複数の水平解像度の計算結果を用いてダスト巻き上げ過程の特性を調べた。これらの計算では、総観規模から小規模までの様々な種類の擾乱が表現されている。ここでは、分布関数を用いてこれらの擾乱に伴うダスト巻き上げを調べ、一般に、解像度が高くなるほどダスト巻き上げ量が大きくなることを示した。これは高い解像度のモデルほど小規模擾乱をより良く表現できることに起因しているものと考えられる。しかし、特に中高緯度においては、低解像度のモデルの方でダスト巻き上げ量がより多い場合があることも示された。これは中高緯度における総観規模擾乱の変動性が低緯度の擾乱の変動性に比べて大きいことによるものと考えられる。

キーワード:惑星大気, スーパーローテーション, ダストストーム, 地球, 火星, 金星